

Permanent Deformation Characteristics of Flexible Pavement Under Palm Oil Freight Truck Loading

Dian M. Setiawan^{1,2*}

¹Department of Civil Engineering,
Universitas Muhammadiyah Yogyakarta, Jl. Brawijaya, Bantul, 55184, INDONESIA

²Zachry Department of Civil and Environmental Engineering,
Texas A&M University, 201 Dwight Look Engineering Building, College Station, Texas, 77843, UNITED STATES

*Corresponding Author

DOI: <https://doi.org/10.30880/ijie.2023.15.02.004>

Received 20 February 2023; Accepted 10 May 2023; Available online 13 June 2023

Abstract: Most of previous studies employed dynamic stability test and Hamburg wheel tracking test to investigate permanent deformation characteristics of asphalt concrete (AC) layer. However, the permanent deformation performance only focuses on the surface course and neglected the influence of middle layer and base course. The present study investigates the permanent deformation characteristics of four (4) different configurations of flexible pavement and analyzes the contribution of AC surface and AC base course to the total permanent deformation of AC layer as the response to various truck's speed, hauling loads, and loading cycles. Finite element modeling was performed to evaluate critical locations below the tire tread of single unit two-axles truck with the greatest magnitude of permanent deformation and to determine the optimum configuration of flexible pavement by considering the linear viscoelastic behavior of two types of AC mixtures. It can be concluded that the largest permanent deformation is measured below the right edge of the outer tire. The contribution of AC surface course on the total permanent deformation due to the increase in truck's speed is only about 14.81% to 16.39%, while the contribution of AC surface course on the total permanent deformation due to the increase in truck's hauling loads as well as the increase in the number of passing trucks is only around 14.76% to 16.44%. On the other hand, the contribution of AC base course on the total permanent deformation due to the increase in truck's speed from is reaching 83.61% to 85.19%, while the contribution of AC base course on the total permanent deformation due to the increase in truck's hauling loads as well as the increase in the number of passing trucks is achieving 83.56% to 85.24%.

Keywords: Asphalt concrete, flexible pavement, freight truck, rutting, permanent deformation

1. Introduction

Indonesia is ranked first based on the quantity of plantation expansion and the rate of oil palm planting, and Riau Province is ranked first with a contribution of 29% to the total national palm oil production [1]. The results of research conducted by Rafli and Buchori [2] describe a significant increase in the area of oil palm plantations, namely 2.15 million hectares (24.12%) of the total area of Riau Province. According to Manurung et al. [3], Riau as the province with the largest oil palm plantations in Indonesia, has an important record where 1,896,662 hectares (ha) or 45.48% of the total area covered by oil palm is indicated to be in forest areas and almost evenly distributed in all urban districts in Riau Provinces, including: Rokan Hilir (392,916 ha), Bengkalis (248,463 ha), Rokan Hulu (241,355 ha), Indragiri Hulu (228,323 ha), Pelalawan (206,857 ha), Kampar (168,144 ha), Indragiri Hilir (139,532 ha), Siak (76,618 ha), and Dumay (73,325 ha) [4]. Oil palm plantations located within the forest area are dominated by smallholder oil palm plantations

*Corresponding author: diansetiawanm@ft.umy.ac.id

which cover 1,832,230 ha, while large (corporate) plantations cover only 64,432 ha.

The production of palm fruit bunches in Riau Province is transported using freight trucks due to the unavailability of a rail network (see Fig. 1). According to a survey conducted by the Public Works Department of Riau Province, 45% of road damage in Riau Province was caused by the overload of vehicles, especially trucks transporting palm oil. The axle load of vehicles that are permitted to pass through the road is 8 tons, but in reality, the axle load of vehicles passing through the roads in Riau Province generally exceeds 75-100% of the permitted axle load weight [5], [6].



Fig. 1 - Palm oil freight truck in Riau, Indonesia [7]

According to Nagy et al. [8], pavement distress is an essential parameter of pavement design. Most pavement distresses are caused by deficiencies in materials, construction, and maintenance. Rutting, also known as permanent deformation (see Fig. 2 and Fig. 3), is considered a primary distress mode in asphalt flexible pavements and has always been a concern in the asphalt pavement industry [9]. Rutting is also one of the typical failure modes of semi-rigid base asphalt pavement in the high-temperature area [10]. The presence of rutting on flexible pavement structure has always been a concern that destructively influences the performance of the pavement by shortening its lifespan and creating a safety hazard for vehicles [11]. Permanent deformation can also lead to severe traffic accidents under some adverse driving circumstances such as rain and curve section [12].

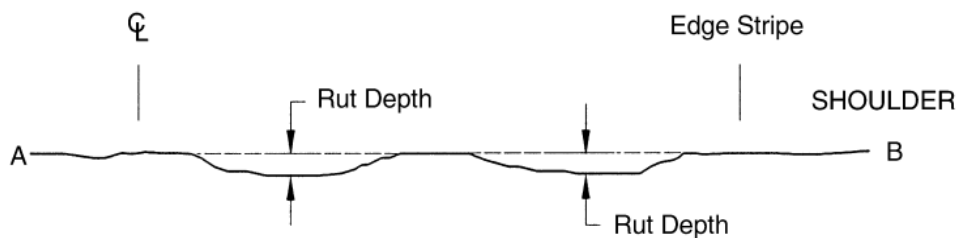


Fig. 2 - Cross-section of rutting or permanent deformation [13]



Fig. 3 - Rutting or permanent deformation in flexible pavement [13]

In rigid pavement, temperature gradients across the concrete slab depth will occur due to the temperature difference between the top and bottom of the PCC layer, which leads to a tendency to curl and differential expansions [14]- [17]. Joshi et al. [18] have demonstrated that, for a given joint spacing and stiff slab thickness, a larger modulus of subgrade response can result in a greater temperature-induced curling stress. In stiff pavement, a higher curling stress might lead to a higher loading and curling stress. Traditional thought, on the other hand, implies that flexible pavements would collapse structurally in one of two ways: deformation due to subgrade failure or fatigue cracking from the bottom up [19]. A longitudinal surface depression in the wheel path is referred to as rutting or permanent deformation. There might be a transverse displacement related to it.

Etheridge et al. [20] employed three distinct types of binders: PG 64-22, PG 67-22, and PG 76-22. While PG 76-22 binders were polymer-modified, PG 64-22 and PG 67-22 were unaltered binders. The PG 76-22 mixtures are thought to have stronger rutting resistances due to their higher modulus, making them more appropriate for usage on higher class roadways. Gopalam et al. [21] discovered that using 2% nano-silica with 6% cement for the subgrade stabilization may minimize rutting in asphalt layer by up to 18-22%, respectively.

The research has also demonstrated that the stiffness of non-asphalt layers and the layer thickness of asphalt pavements affect how they respond to fatigue [22]- [25]. As a result, a thorough performance evaluation of fatigue behaviors takes into account the structural reaction of the entire pavement system. To identify system features, linear elastic structural response models have been created, such as the WinJULEA platform utilized in the Mechanistic-Empirical Pavement Design Guide (MEPDG) [25]. According to Eslaminia et al. [26], current research is going toward linear viscoelastic analysis of multilayer systems since it is thought to be more reflective of pavement response to stress and strain. With a mechanistic approach in the ABAQUS program, Park et al. [27] examined predictions for various materials of AC mixtures. This method has shown promise in matching field performance to simulated performance.

Due to the involvement of both material technology and a permanent deformation mechanism, the problem of rutting of the AC layer in flexible pavement is a broad one. The amount of fatigue and bending experienced by the pavement's upper layers varies according to thickness [28]- [30]. Fatigue degradation is more likely to affect the asphalt foundation than permanent deformations. While the initiation of fatigue fractures in this layer is likely when there is insufficient interlayer bonding of asphalt layers with propagation of the crack occurring in the base, the binder course is already exposed to irreversible deformation and can also be susceptible to low-temperature damage [28], [31]- [34]. In the event of loss of adhesion or the beginning of propagation from the lower layers, the surface course is vulnerable to damage from the bottom. Due to its elevated location, it is also visibly susceptible to "top to bottom" cracks.

Prior research used the Hamburg wheel tracking test and dynamic stability test to examine rutting features of flexible pavement [35]- [39]. However, because the asphalt concrete (AC) mixtures were placed in a rigid steel or hard plastic mold, the middle layer, bottom layer, and base course had no bearing on the rutting performance, which reduced it to a characteristic of the asphalt concrete material rather than the pavement structure. In addition, it is difficult to find research that discuss the contribution of AC surface and AC base course on the total permanent deformation of the AC layer as the response to the various combination of truck's speed, hauling loads, and loading cycles. Performing the field testing in order to measure the permanent deformation development within the AC layer is complex and time consuming.

To overcome these problems, this research investigates the permanent deformation characteristics of four (4) different configurations of flexible pavement, as well as analyzes the contribution of AC surface and AC base course to the total permanent deformation of AC layer as the response to various truck's speed, hauling loads, and loading cycles. Finite element numerical modeling was constructed to evaluate the greatest magnitude of permanent deformation within several critical locations below the tire tread of single unit two-axles truck and to determine the optimum configuration of flexible pavement with certain thickness of AC surface and AC base courses by considering linear viscoelastic behavior of two (2) variant of AC materials.

2. Methods

2.1 Flexible Pavement Structural Configuration

Four (4) configurations of flexible pavement with the width of 3000 mm were developed and considered in this study (see Fig. 4). As shown in Fig. 4(a), first configuration consists of AC Type 1 as AC surface course (100 mm), AC Type 2 as AC base course (200 mm), followed by sub-base (450 mm) and subgrade layer (900 mm). Second configuration, illustrated in Fig. 4(b), includes the AC Type 2 as surface layer (100 mm), AC Type 1 as base layer (200 mm), followed by sub-base (450 mm) and subgrade layer (900 mm). Third configuration comprise of AC Type 1 (300 mm), sub-base (450 mm), and subgrade layer (900 mm), presented in Fig. 4(c). Finally, Fig. 4(d) depicted fourth configuration, constructed with AC Type 2 (300 mm), sub-base (450 mm), and subgrade layer (900 mm).

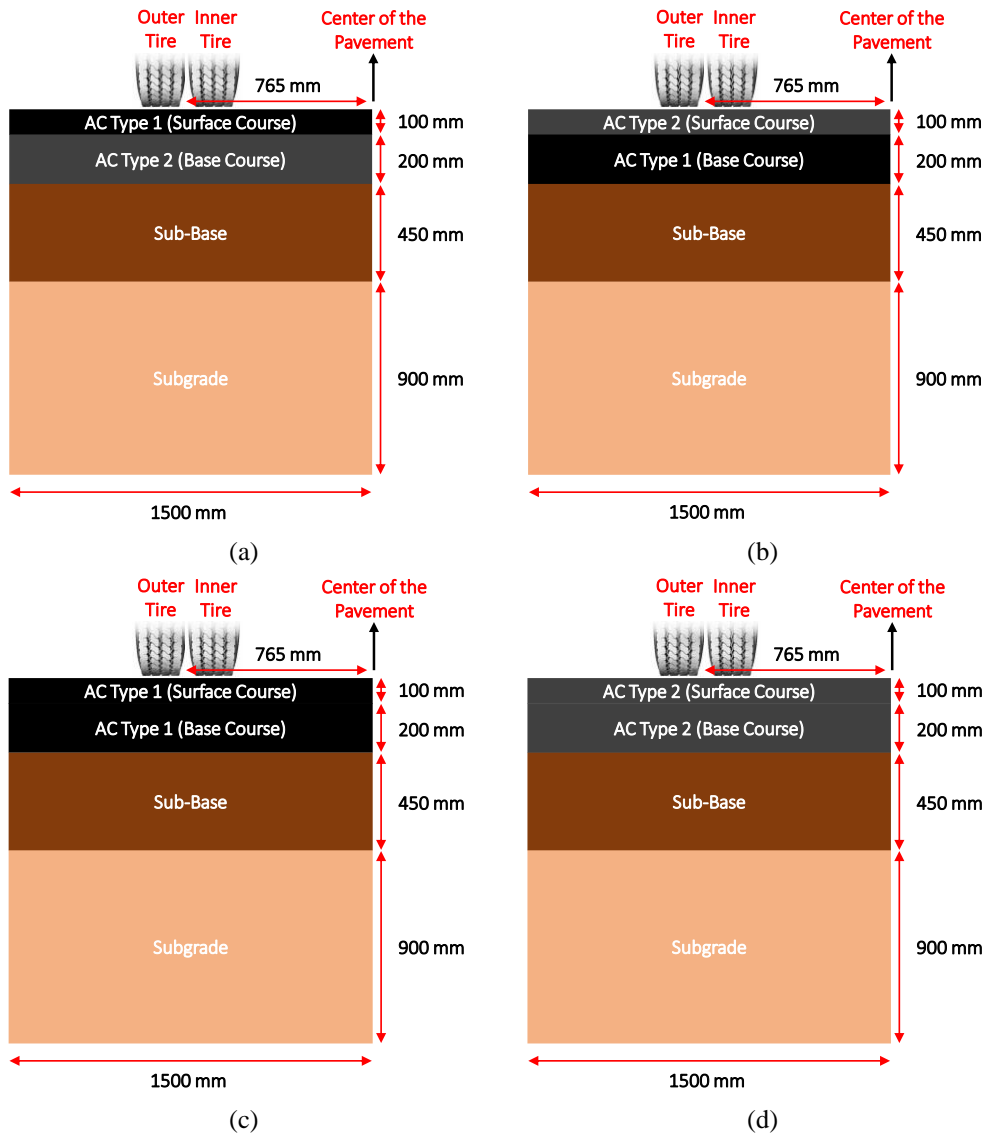


Fig. 4 - Four different flexible pavement structural configuration; (a) configuration 1; (b) configuration 2; (c) configuration 3; (d) configuration 4

2.2 Loading System from Freight Truck

The wheel configuration based on a single unit two-axles truck load was applied to the interior of the flexible pavement, as shown in Fig. 5. The variations of loading systems from freight trucks were based on three different running speeds (40, 60, and 80 kph), three different hauling loads (10, 25, and 36 tons/truck), and two different loading cycles (5000 and 10,000 times). Therefore, in total there were 9 model variations (see Table 1).

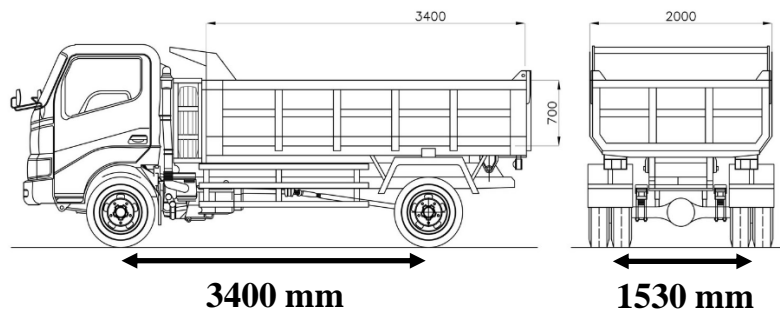


Fig. 5 - Single unit two-axles truck load

Table 1 - Loading systems based on combination of freight truck's speed, axle load, and loading cycles

Case	Speed (km/h)	Axle Load (Tons)	Loading Cycles	Truck's Capacity (Tons/Truck)	Number of Truck	Hauling Capacity (Tons)
1	40					
2	60	5,000	5000	10,000	5000	50,000
3	80					
4	40					
5	60	12,500	10,000	25,000	10,000	250,000
6	80					
7	40					
8	60	18,000	10,000	36,000	10,000	360,000
9	80					

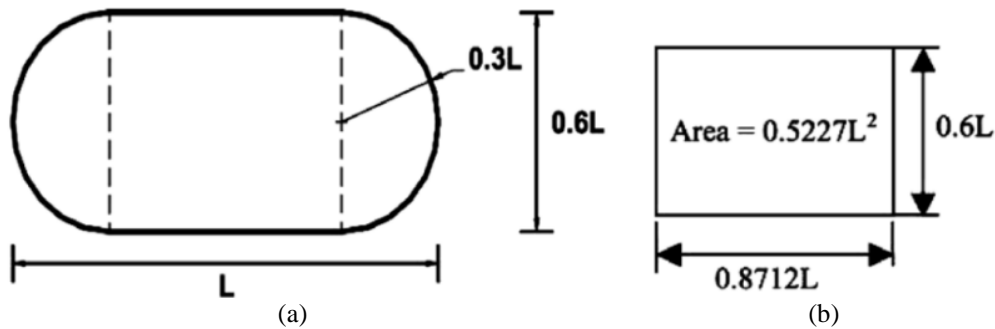
**Fig. 6 - (a) Contact area between tires and the pavement surface; (b) equivalent contact area [14], [23]**

Fig. 6 presents the contact area between tires and the pavement surface and its equivalent contact area. As shown in Fig. 6, the freight truck load was in the form of cyclic pressure load. Since L is 0.388 m, one (1) wheel has the rectangular area conversion of $0.5227 L^2$, with a length of 0.338 m and a width of 0.234 m.

2.3 Material Properties

The material properties of AC Type 1 and AC Type 2 were obtained from Lee et al. [40], considering the linear elastic and viscoelastic characteristics. The material properties of unbound aggregate of sub-base and soil subgrade layer was acquired from Indonesian Standard and Regulation. Table 2 presents the elastic parameters of the materials considered in this study.

Table 2 - Material properties

Structural Layer	Mass Density, ρ (kg/m ³)	Elastic Modulus, E (GPa)	Poisson's Ratio, ν
AC Type 1 [40]	2345.35	25,2	0.35
AC Type 2 [40]	2345.35	22,9	0.35
Sub-Base	1900	0.12	0.30
Subgrade	2000	0.06	0.25

2.4 Construction of The Model

Fig. 7 depicts the results of flexible pavement structural configurations in 2D model using ABAQUS software. Element 3-node linear plane strain triangle, CPE3, was selected for AC surface course (structured) and AC base course (free). In addition, element 4-node bilinear plane strain quadrilateral, CPE4, was selected for sub-base (structured) and subgrade (structured) layer.

The mesh size of 0.025 m x 0.025 m was created below tire footprints, followed by 0.025 m x 0.05 for the first AC layer, 0.05 m x 0.05 m for the second AC layer, and 0.05 m x 0.1 m for both the sub-base and subgrade of the flexible pavement. Furthermore, the red, yellow, and blue dots in Fig. 7 are the location of measuring nodes to obtain the magnitude of vertical displacement at the surface of the 1st AC layer or AC surface course (nodes I, II, III, IV, V, and VI), at the interface of the 1st and 2nd AC layer (nodes A, B, C, D, E, and F), and at the bottom of the 2nd AC layer or AC base course (nodes 1, 2, 3, 4, 5, and 6), respectively. To simplify the model, the interaction of each layer is considered as glued.

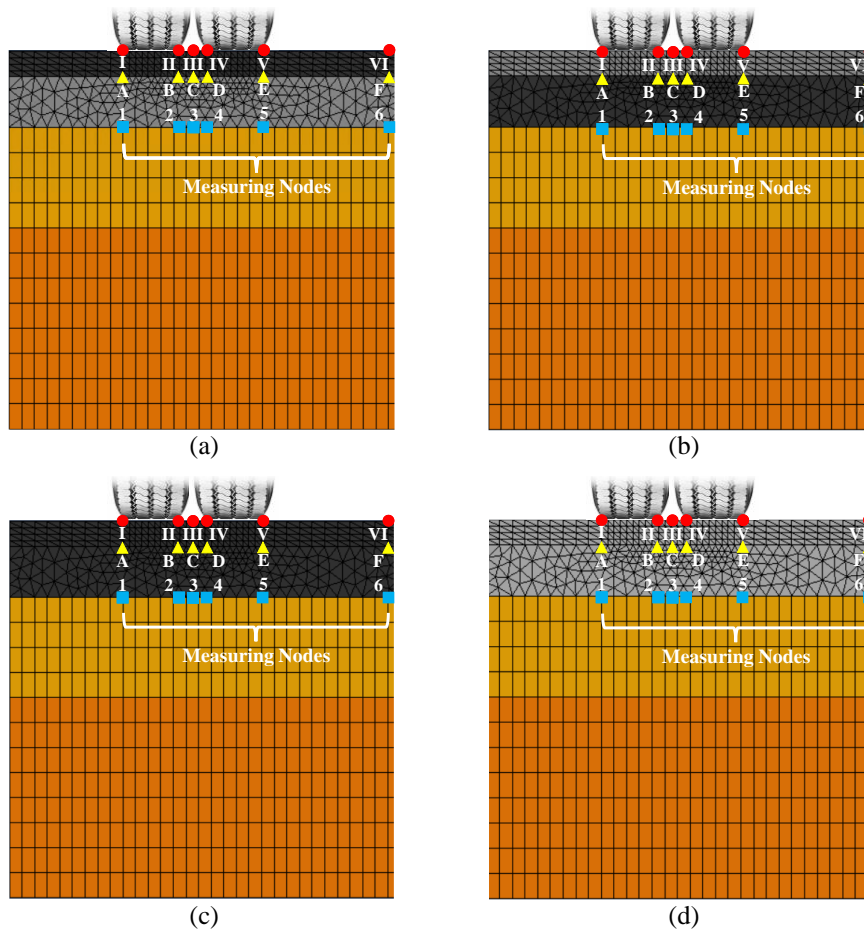
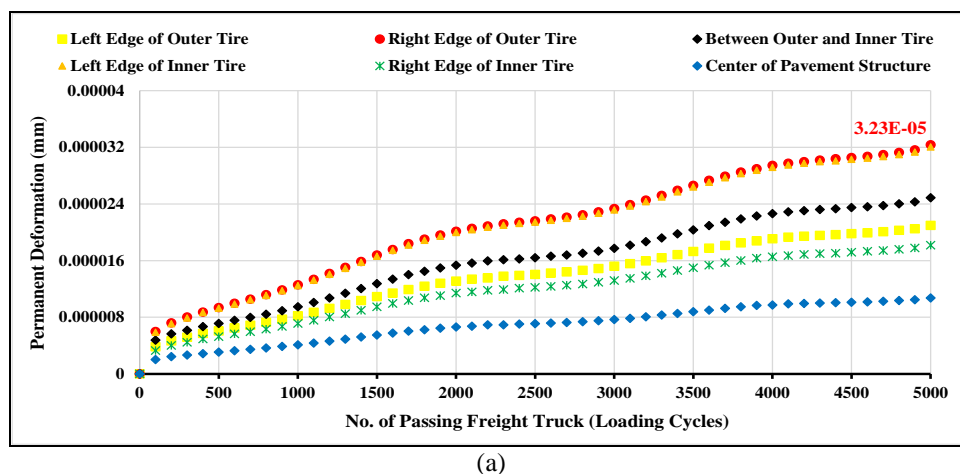


Fig. 7 - Flexible pavement in 2D model and the measuring nodes; (a) configuration 1; (b) configuration 2; (c) configuration 3; (d) configuration 4

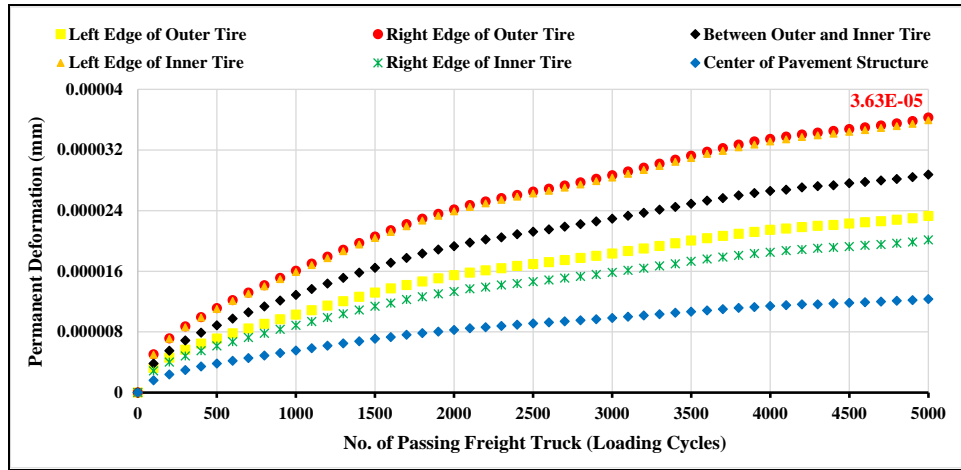
3. Results and Discussion

3.1 Permanent Deformation in Critical Locations Within AC Layer

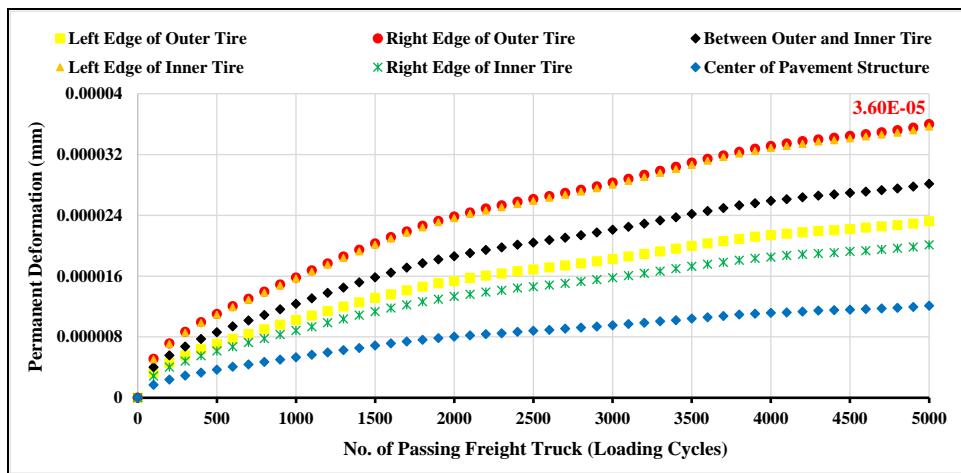
As part of the pavement design and analysis process, it is important to detect the critical location within the AC layer with the largest permanent deformation, so that we can understand the relationship between the performance of the AC layer structure due to the vehicle loadings as the function of the speed, loads magnitudes, and loading cycles. Therefore, Fig. 8 illustrates the growth of permanent deformation at six (6) different locations within the AC layer due to 1st Case (10 tons/truck, 40 kph, 5000 loading cycles) in configuration 1 (see Fig. 8(a)), 2 (see Fig. 8(b)), 3 (see Fig. 8(c)), 4 (see Fig. 8(d)).



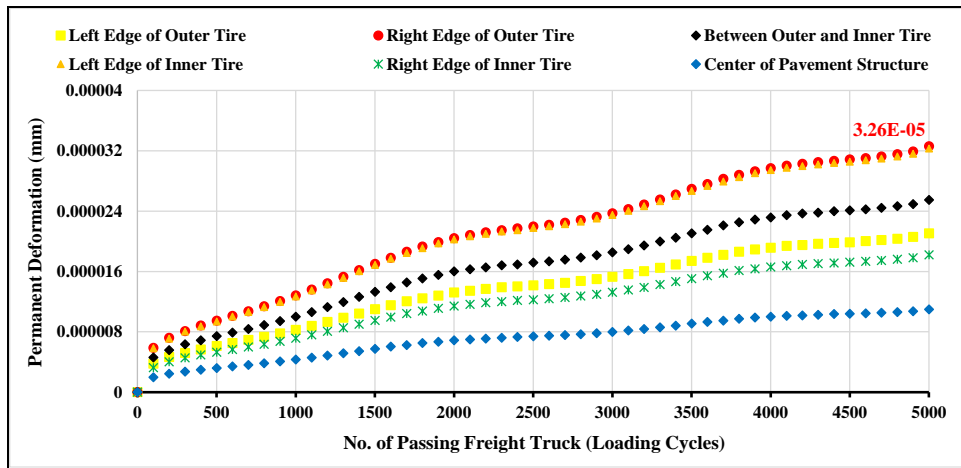
(a)



(b)



(c)



(d)

Fig. 8 - Permanent deformation at six (6) different locations within the AC layer due to 1st case (10 tons/truck, 40 kph, 5000 loading cycles); (a) configuration 1; (b) configuration 2; (c) configuration 3; (d) configuration 4

Fig. 8 confirmed that all four (4) configurations of the flexible pavements provide similar trend, where the largest permanent deformation is measured and located below the right edge of the outer tire, followed by permanent deformation below the left edge of the inner tire, between the outer and inner tire, below the left edge of the outer tire, below the right edge of the inner tire, and parallel to the center of the pavement structure. In addition, in terms of the 1st Case, where the loading systems were due to the combination of the truck’s speed of 40 kph, truck’s hauling loads of 10 tons/truck, and the number of loading cycles or the passing trucks of 5000 trucks, the flexible pavement of configuration 1 with the AC Type 1 served as AC surface course and the AC Type 2 served as AC base course produce

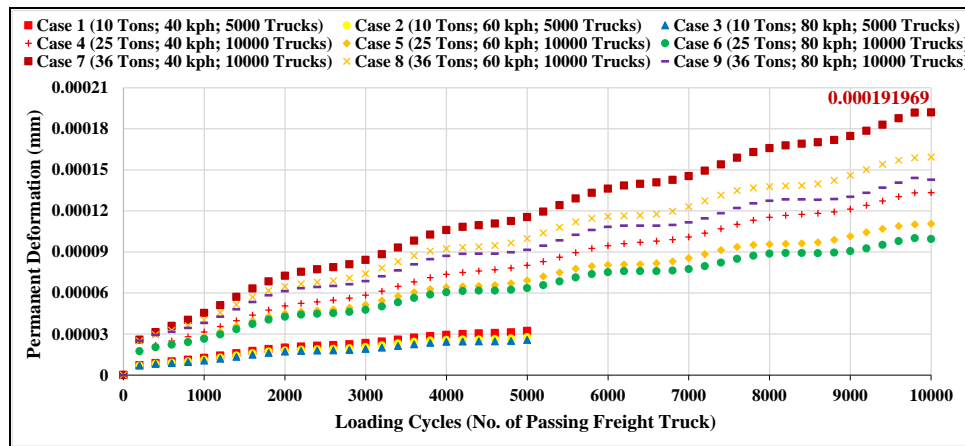
the smallest permanent deformations among others configurations, followed by configuration 4 (AC Type 2 served as both AC surface and AC base course), configuration 3 (AC Type 1 served as both AC surface and AC base course), and configuration 2 (AC Type 2 served as AC surface course and the AC Type 1 served as AC base course).

However, Fig. 8 only shows the behavior of the flexible pavement due to the considerably low speeds, light hauling loads, and small loading cycles. Therefore, it is essential to evaluate the largest permanent deformations of the AC layer at the same critical location found in Fig. 8, below the right edge of the outer tire, by considering other cases (faster truck's speed, heavier truck's hauling loads, and higher loading cycles) that have been detailed in Table 1.

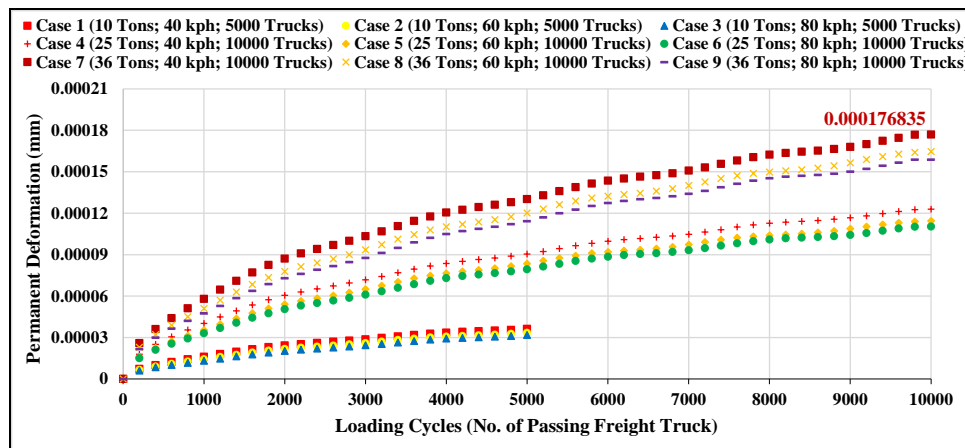
3.2 Effect of Freight Truck's Hauling Loads, Speed, and Loading Cycles On Permanent Deformation

Due to this increased traffic, the rutting of flexible pavement has become major distress, which is leading to the permanent deformation of the pavement [41]. Liu & Gu [10] concluded that high temperature and heavy axle loads greatly influenced rutting development: tested road was loaded 360,000 times at high temperature, contributing 50% to accumulated rutting; In simulated results, rutting deformation increased by 90.7% under the condition of 50% overload under high temperature seasons. In this study, Fig. 9 depicts the largest permanent deformation of AC layer in each configuration of the flexible pavement for all cases (case 1 through 9) as the combination of truck's speed, hauling loads, and loading cycles.

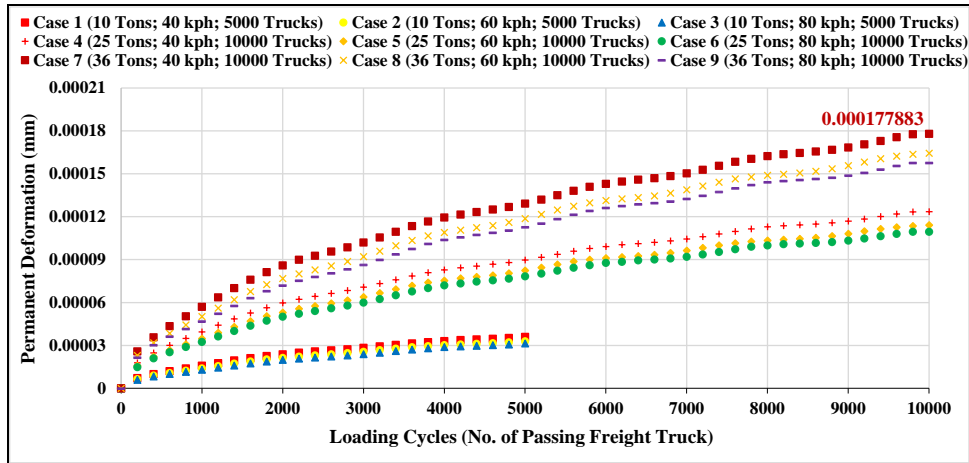
As shown by Fig. 9, all four (4) configurations of the flexible pavements provide similar trend, where the largest permanent deformation of the AC layer is produced by the loading systems according to the case 7 (truck's hauling loads of 36 tons/truck, truck's speed of 40 kph, and truck's loading cycles of 10,000 times), followed by the permanent deformation of the AC layer produced by the loading systems according to the case 8, 9, 4, 5, 6, 1, 2, and 3, respectively. In addition, flexible pavement with configuration 2 (AC Type 2 served as AC surface course and the AC Type 1 served as AC base course) has the smallest permanent deformation especially due to the case 7 (see Fig. 9(b)), followed by configuration 3 (see Fig. 9(c)), configuration 4 (see Fig. 9(d)), and configuration 1 (see Fig. 9(a)), respectively. However, different conditions are shown by other cases.



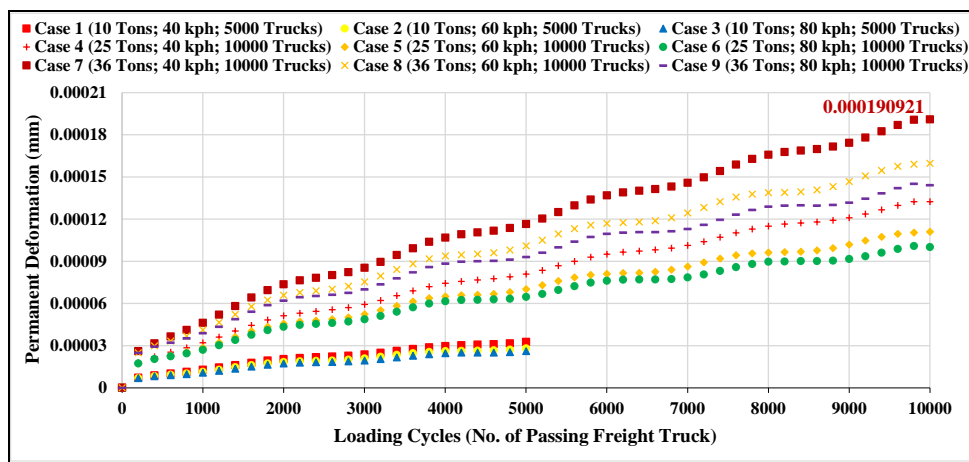
(a)



(b)



(c)



(d)

Fig. 9 - Largest permanent deformation of AC layer for all cases as the combination of truck’s speed, hauling loads, and loading cycles; (a) configuration 1; (b) configuration 2; (c) configuration 3; (d) configuration 4

In the case of the shape of the curve of the permanent deformation development, configuration 1 (see Fig. 9(a)) is identical with configuration 4 (see Fig. 9(d)), and configuration 2 (see Fig. 9(b)) is identical with configuration 3 (see Fig. 9(c)). In configuration 1 and 4, the growth of the permanent deformation is increase uniformly until 10,000 loading cycles. In other side, the growth of the permanent deformation in configuration 2 and configuration 3 is significantly increase up to 2000 loading cycles, and then steadily increase with flatter curve until 10,000 loading cycles. Besides, configurations 1 and 4 (see Fig. 9(a) and Fig. 9(d)) have three different colonies or groups of curves that represents three different permanent deformation development, which are case 1, 2, and 3 as 1st group, case 4, 5, and 6 as 2nd group, and case 7, 8, and 9 as 3rd group. Each group has the same magnitude of truck’s hauling loads and loading cycles but different truck’s speeds. In other words, the effect of truck’s speed in each group in configuration 1 and 4 is not significant. However, the curves that represent nine (9) permanent deformation development from nine (9) different cases appear in a more scattered position in configuration 2 and 3 (see Fig. 9(b) and Fig. 9(c)). In other words, truck’s speed has significant effect on the growth of the permanent deformation of AC layer in configuration 2 and 3.

In fact, it can be predicted that at certain level of loading cycles (> 10,000 loading cycles), the magnitude of permanent deformation of AC layer in configuration 2 and 3 due to case 4 (25 tons/truck, 40 kph, 10,000 loading cycles) will overtake the magnitude of permanent deformation of AC layer due to case 9 (36 tons/truck, 80 kph, 10,000 loading cycles), as presented in Fig. 9(b) and Fig. 9(c). If this is the case, we can conclude that reducing the truck’s speed 2 times slower from 80 kph to 40 kph will increase the risk of the occurrence as well as the magnitude of the permanent deformation of AC layer after higher number of loading cycles (in this study each loading cycles is equal to the number of passing trucks), even though the truck’s hauling loads have been decreased 30% from 36 tons/truck to 25 tons/truck. Also, as expected, the behavior of AC layer as a viscoelastic material in terms of permanent deformation is prone to the slow speeds and heavy loads of vehicle.

3.3 Contribution of AC Surface and AC Base Course On Permanent Deformation

After obtaining the fact that case 7 causes the largest permanent deformation of AC layer in all configurations of flexible pavement discussed in this study, the next stage is evaluating the contribution of AC surface and AC base course on the magnitude of total permanent deformation of AC layer. Fig. 10 and Fig. 11 present the permanent deformation of AC surface and AC base course in all configurations of flexible pavement, respectively, because of truck's speeds variation, 40, 60, and 80 kph, but with the same magnitude of truck's hauling loads and loading cycles, 36 tons/truck and 10,000 times (case 7, 8, and 9).

As expected, Fig. 10 and Fig. 11 confirm that the slower the freight truck's speed, the larger the permanent deformation of both AC surface and AC base course in all configurations of flexible pavement. Besides, even though configuration 4 produce the largest permanent deformation of AC surface course (see Fig. 10) among other configuration due to the loading systems in case 7 (36 tons/truck, 40 kph, and 10,000 loading cycles), however, it shows the most significant reduction of permanent deformation because of the increase in truck's speed from 40 kph to 60 kph (case 8) and 80 kph (case 9), respectively. In other side, even though configuration 1 has the largest permanent deformation of AC base course (see Fig. 11) among other configuration due to the loading systems in case 7 (36 tons/truck, 40 kph, and 10,000 loading cycles), however, it shows the most considerable decrease of permanent deformation because of the increase in truck's speed from 40 kph to 60 kph (case 8) and 80 kph (case 9), respectively.

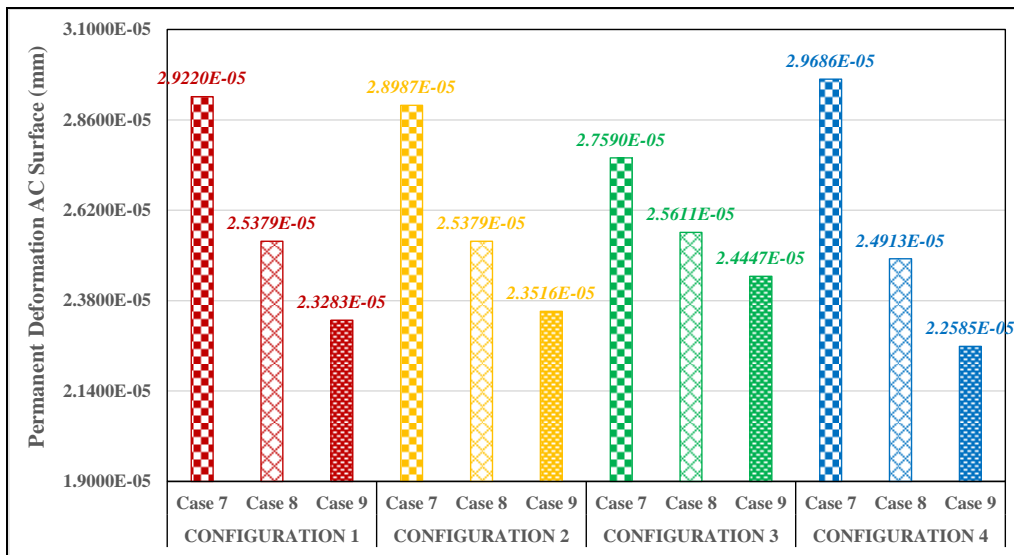


Fig. 10 - Permanent deformation of AC surface course in all configurations of flexible pavement because of loading systems in case 7, 8, and 9

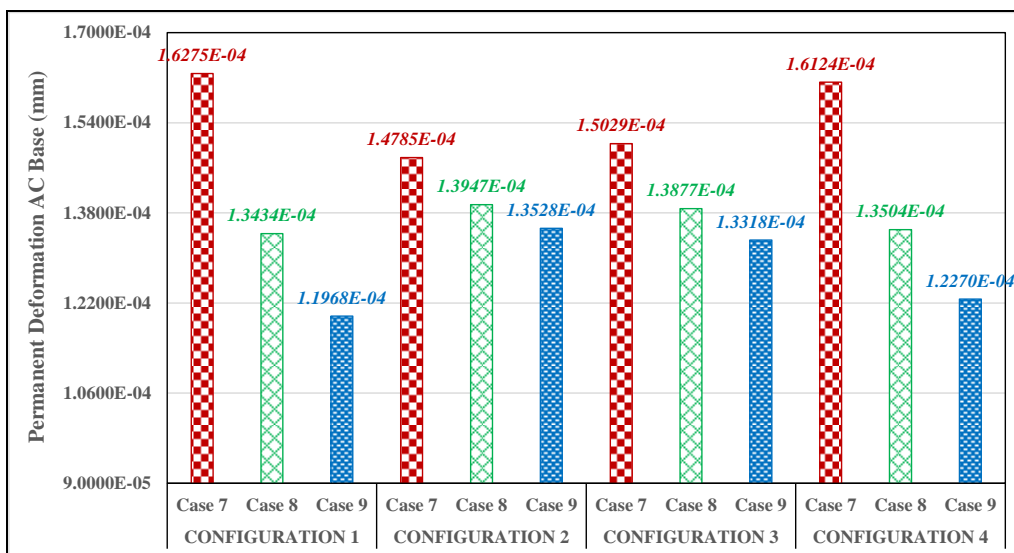


Fig. 11 - Permanent deformation of AC base course in all configurations of flexible pavement because of loading systems in case 7, 8, and 9

Fig. 12 and Fig. 13 present the permanent deformation of AC surface and AC base course in all configurations of flexible pavement, respectively, because of the difference in the magnitude of truck’s hauling loads (10, 25, and 36 tons/truck) and loading cycles (5000 and 10,000 times), but with the same truck’s speed, 40 kph (case 1, 4, and 7).

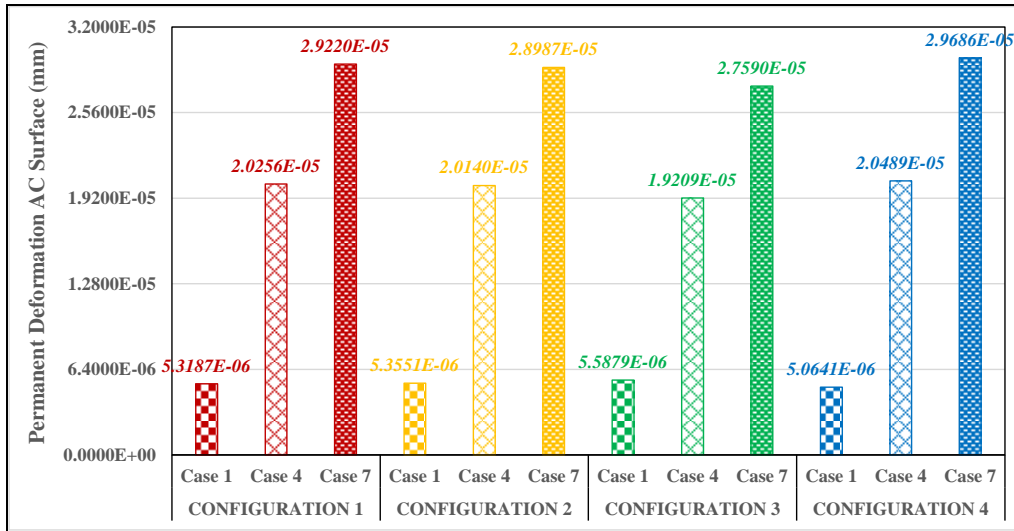


Fig. 12 - Permanent deformation of AC surface course in all configurations of flexible pavement because of loading systems in case 1, 4, and 7

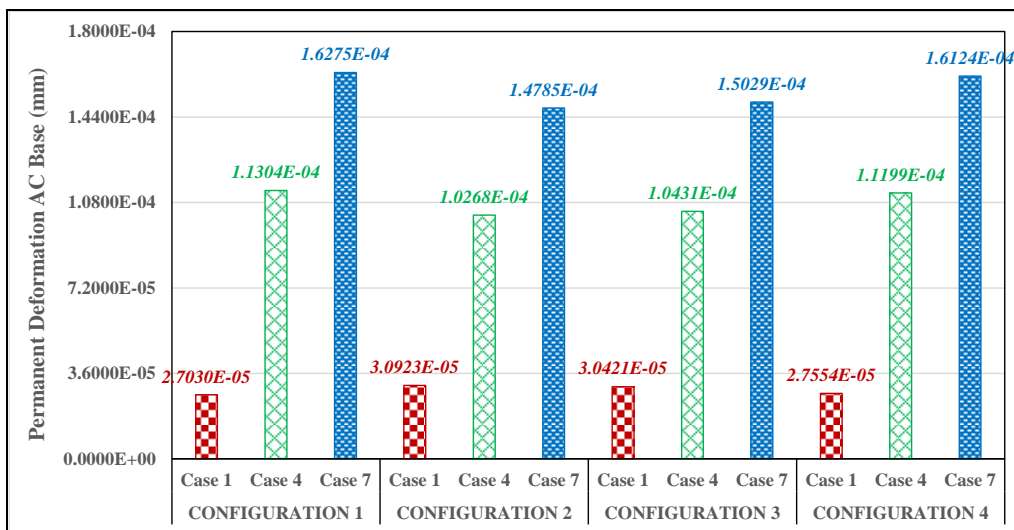


Fig. 13 - Permanent deformation of AC surface course in all configurations of flexible pavement because of loading systems in case 1, 4, and 7

As expected, Fig. 12 and Fig. 13 confirm that the heavier the freight truck’s hauling loads and the higher the loading cycles, the larger the permanent deformation of both AC surface and AC base course in all configurations of flexible pavement. Also, even though configuration 4 produce the largest permanent deformation of AC surface course (see Fig. 12) among other configuration due to the loading systems in case 7 (36 tons/truck, 40 kph, and 10,000 loading cycles), however, it exhibits the most considerable reduction of permanent deformation because of the decrease both in truck’s loading cycles [from 10,000 to 5000] and in truck’s hauling loads [(from 36 tons/truck to 25 tons/truck (case 4) and 10 tons/truck (case 1)], respectively. In other side, even though configuration 1 has the largest permanent deformation of AC base course (see Fig. 13) among other configuration due to the loading systems in case 7 (36 tons/truck, 40 kph, and 10,000 loading cycles), however, it shows the most substantial reduction of permanent deformation because of the decrease both in truck’s loading cycles [from 10,000 to 5000] and in truck’s hauling loads [(from 36 tons/truck to 25 tons/truck (case 4) and 10 tons/truck (case 1)], respectively.

Fig. 14 illustrates the total permanent deformation of AC layer in all configurations of flexible pavement due to truck’s speeds variation, 40, 60, and 80 kph, but with the same magnitude of truck’s hauling loads and loading cycles, 36 tons/truck and 10,000 times (case 7, 8, and 9). Fig. 15 provides the total permanent deformation of AC layer in all configurations of flexible pavement due to the difference in the magnitude of truck’s hauling loads (10, 25, and 36

tons/truck) and loading cycles (5000 and 10,000 times), but with the same truck's speed, 40 kph (case 1, 4, and 7). It can be observed that the increase of truck's speed from 40 kph to 60 kph (50% higher) and from 60 kph to 80 kph (33% higher) only reduce the total permanent deformation around 6.8-16.8% and 3.7-10.5%, respectively (see Fig. 14). However, the decrease of truck's hauling loads from 36 tons/truck to 25 tons/truck (30% lighter) and from 25 tons/truck to 10 tons/truck (60% lighter) can reduce the total permanent deformation around 30.6% and 70.5-75.7%, respectively (see Fig. 15).

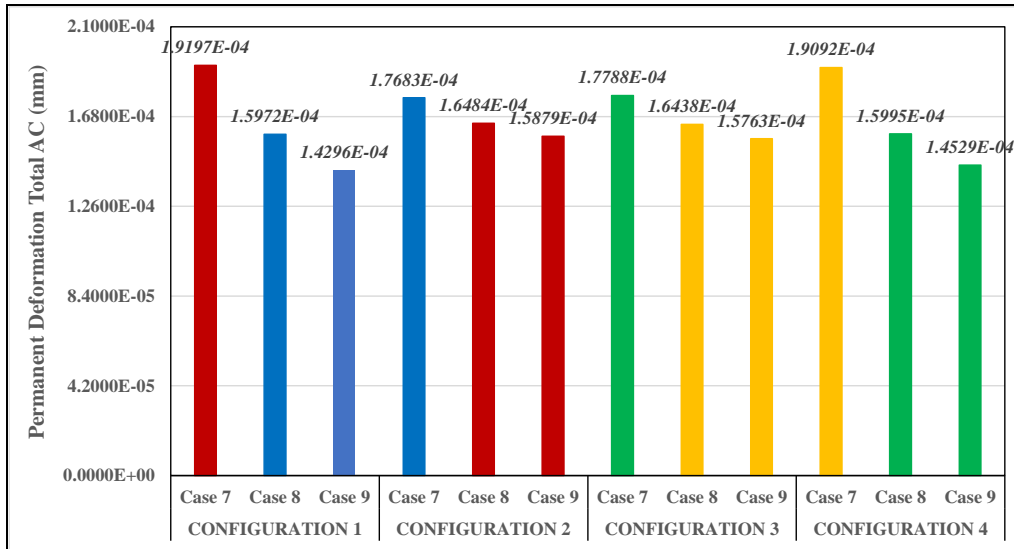


Fig. 14 - Total permanent deformation of AC layer in all configurations of flexible pavement due to loading systems in case 7, 8, and 9

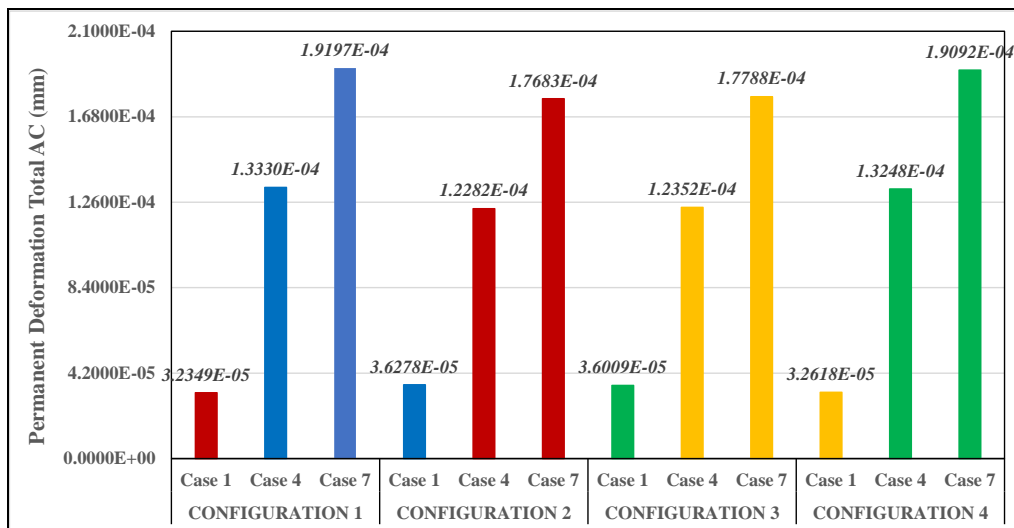


Fig. 15 - Total permanent deformation of AC layer in all configurations of flexible pavement due to loading systems in case 1, 4, and 7

As shown in Fig. 16, percentage contribution of AC surface on the total permanent deformation due to the case 7, 8, and 9 is showing an increase trend in configuration 1 (15.22%, 15.89%, and 16.29%), a decrease trend in configuration 2 (16.39%, 15.40%, and 14.81%), and fluctuations trend in configuration 3 (15.51%, 15.58%, and 15.51%) and configuration 4 (15.55%, 15.57%, and 15.54%). In addition, percentage contribution of AC base on the total permanent deformation due to the loading systems in case 7, 8, and 9 is showing a decrease trend in configuration 1 (84.78%, 84.11%, and 83.71%), an increase trend in configuration 2 (83.61%, 84.60%, and 85.19%), and fluctuations trend in configuration 3 (84.49%, 84.42%, and 84.49%) and configuration 4 (84.45%, 84.43%, and 84.46%). Fig. 17, on the other hand, represents the fluctuation in the percentage contribution of both AC surface and AC base courses on the total permanent deformation due to the loading systems in case 1, 4, and 7.

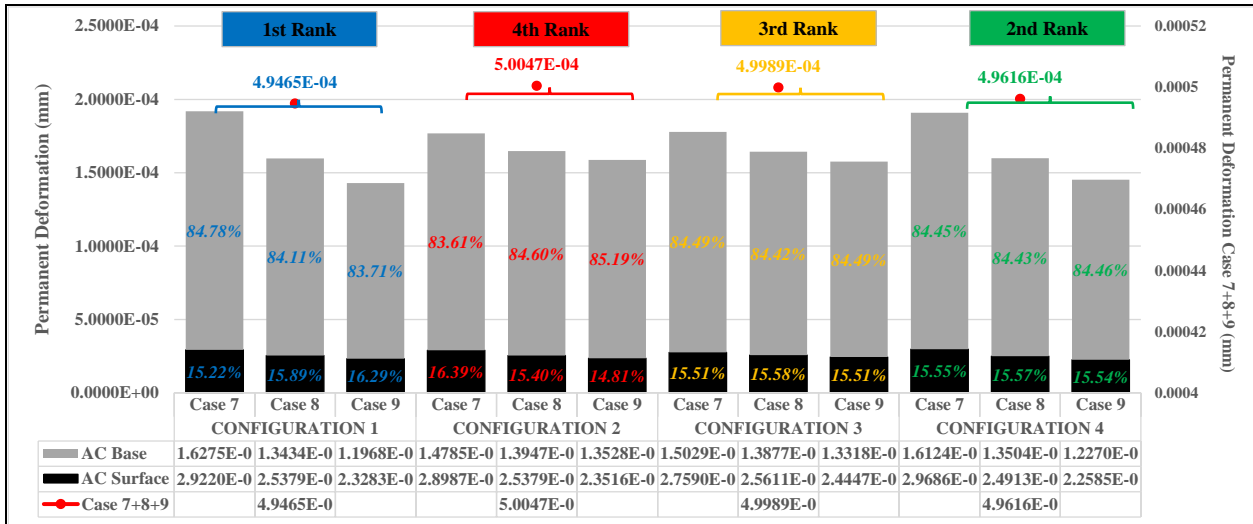


Fig. 16 - Contribution of AC surface and AC base course on total permanent deformation of AC layer in all configurations of flexible pavement due to loading systems in case 7, 8, and 9

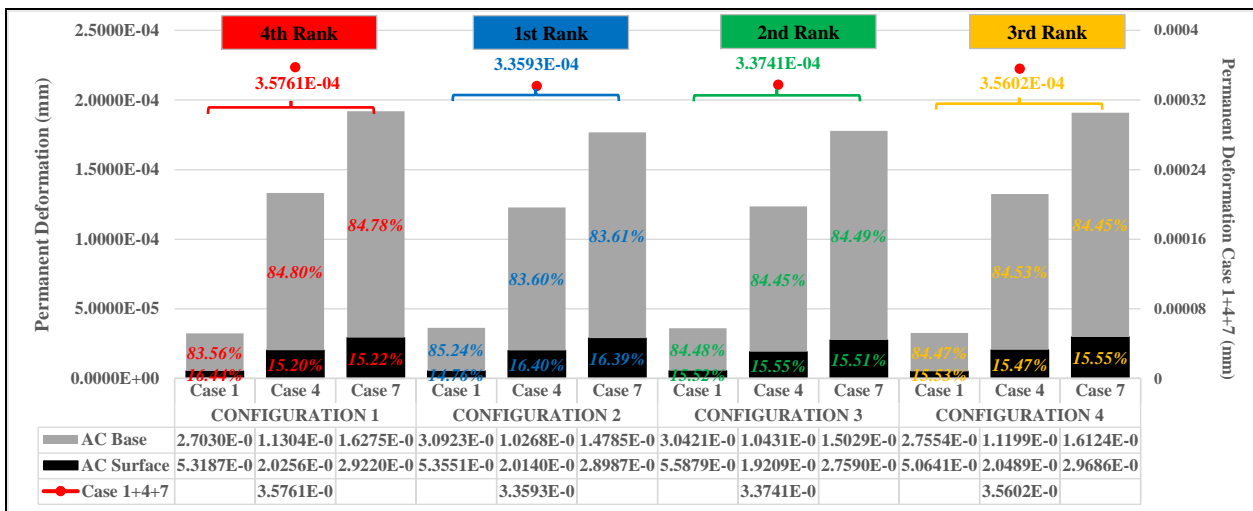


Fig. 17 - Contribution of AC surface and AC base course on total permanent deformation of AC layer in all configurations of flexible pavement due to loading systems in case 1, 4, and 7

The next stage is the analysis of the numerical model results to determine the optimum configuration of flexible pavement that produce the minimum total permanent deformation of AC layer as combination of the magnitude of permanent deformation due to the loading systems in case 7, 8, and 9 (variations in truck’s speed, which are 40, 60, and 80 kph, see Fig. 16) as well as in case 1, 4, 7 (variations in truck’s hauling loads, which are 10, 25, and 36 tons/truck, and in truck’s loading cycles, which are 5000 and 10,000 times, see Fig. 17). Based on Fig. 16, the most optimum configuration of flexible pavement is configuration 1, followed by configuration 4, configuration 3, and configuration 2. On the other hand, Fig. 17 shows that the most optimum configuration of flexible pavement is configuration 2, followed by configuration 3, configuration 4, and configuration 1.

4. Conclusions

This research utilized the numerical modeling of four (4) different configurations of flexible pavement to evaluate the contribution of AC surface and AC base course on the total permanent deformation of the AC layer as the response to the various combination of truck’s speed (40, 60, and 80 kph), hauling loads, and loading cycles.

It can be concluded that the largest permanent deformation is measured and located below the right edge of the outer tire. Moreover, it can be predicted that at certain amount of loading cycles (> 10,000 loading cycles), the total permanent deformation of AC layer in configuration 2 and 3 due to case 4 (25 tons/truck, 40 kph, 10,000 loading cycles) will overtake the magnitude of permanent deformation of AC layer due to case 9 (36 tons/truck, 80 kph, 10,000 loading cycles). In other words, reducing the truck’s speed 2 times slower from 80 kph to 40 kph will increase the magnitude of total permanent deformation of AC layer after higher number of passing trucks, even though the truck’s

hauling loads have been decreased 30% from 36 tons/truck to 25 tons/truck. Future research should be conducted to with higher loading cycles, for example 50,000 times, to capture the more data and information regarding the growth and the development of total permanent deformation of AC layer and their response to the various loading systems.

The percentage contribution of AC surface course on the total permanent deformation due to the increase in truck's speed from 40 kph to 60 kph and 80 kph is only about 14.81% to 16.39%, while the percentage contribution of AC surface course on the total permanent deformation due to the increase in truck's hauling loads from 10 tons/truck to 25 tons/truck and 36 tons/truck as well as the increase in the number of passing trucks from 5000 to 10,000 trucks is only around 14.76% to 16.44%. On the other hand, the proportion contribution of AC base course on the total permanent deformation due to the increase in truck's speed from 40 kph to 60 kph and 80 kph is reaching 83.61% to 85.19%, while the percentage contribution of AC base course on the total permanent deformation due to the increase in truck's hauling loads from 10 tons/truck to 25 tons/truck and 36 tons/truck as well as the increase in the number of passing trucks from 5000 to 10,000 trucks is achieving 83.56% to 85.24%.

If the stakeholders prefer to increase the truck's speed in order to increase the hauling capacity of the freight truck and at the same time to minimize the magnitude of the permanent deformation in AC layer, so it is suggested to apply the flexible pavement with configuration 1, where the AC Type 1 served as AC surface layer and AC Type 2 served as AC base layer. Furthermore, if the stakeholders prefer to increase the truck's hauling loads and loading cycles in order to increase the hauling capacity of the freight truck and at the same time to minimize the magnitude of the permanent deformation in AC layer, then it is suggested to apply the flexible pavement with configuration 2, where the AC Type 2 served as AC surface layer and AC Type 1 served as AC base layer.

References

- [1] Hidayah N., Dharmawan A. H. & Barus B. (2016). The expansion of palm oil plantation and changes of rural social ecology. *Sodality, Jurnal Sosiologi Pedesaan*, 4(3), 249-256. <https://doi.org/10.22500/sodality.v4i3.14434>
- [2] Rafli M. & Buchori I. (2022). Dampak ekspansi kebun kelapa sawit terhadap kondisi jasa lingkungan Provinsi Riau (In Bahasa Indonesia). *Jurnal Pembangunan Wilayah dan Kota*, 18(2), 98-111. <https://doi.org/10.14710/pwk.v18i2.21229>
- [3] Manurung G. M. E., Siregar Y. I., Syahza A., Suwondo S., Nofrizal N., Apriyanto M. & Mustofa R. (2022). Keberlanjutan dan Tantangan Perkebunan Kelapa Sawit Rakyat dalam Bingkai Tata Kelola Kehutanan. *Taman Karya, Indonesia*.
- [4] Pusat Pengendalian Pembangunan Ekoregion Sumatera (2020). Hasil Verifikasi Lapangan (Ground Check) Kegiatan Inventarisasi Daya Dukung Daya Tampung Provinsi Riau Untuk Perkebunan Kelapa Sawit. Kementerian Lingkungan Hidup dan Kehutanan, Indonesia.
- [5] Sentosa L. & Roza A. W. (2012). Analisis dampak beban overloading kendaraan pada struktur rigid pavement terhadap umur rencana perkerasan (Studi kasus ruas jalan simp lago - Sorek KM 77 S/D 78). *Jurnal Teknik Sipil*, 19(2), 161-168.
- [6] Firdaus F. (1999). Analisis dampak negatif beban berlebih (overload) terhadap perkerasan jalan. *Prosiding Konferensi Regional Teknik Jalan Ke-6 Wilayah Barat, Indonesia*.
- [7] Go Riau (2013). Truk sawit penyebab utama rusaknya jalan di Siak. <https://www.goriau.com/berita/baca/truk-sawit-penyebab-utama-rusaknya-jalan-di-siak.html>
- [8] Nagy A. A., El-Maaty A. E. A. & Hashim I. H. (2023). Evaluation of maintenance and rehabilitation treatments on long-term asphalt pavement performance. *Engineering Research Journal*, 46(1), 65-81.
- [9] Bastola N. R., Souliman M. I. & Vechione M. (2023). Preliminary study on rutting performance of pavement structures under the effect of future autonomous vehicle movements. *Innovative Infrastructure Solutions*. <https://doi.org/10.1007/s41062-022-01024-2>
- [10] Liu Z. & Gu X. (2023). Analysis for rutting development and evolution rules of asphalt pavement based on accelerated pavement test. *The Transportation Research Board (TRB) 102nd Annual Meeting, United States*.
- [11] Hatoum A., Khatib J., Barraj F. & Elkordi A. (2022). Assessing the influence of overweight axles on rutting lives in flexible pavements using parametric survival analysis. *BAU Journal - Science and Technology*. <https://www.doi.org/10.54729/CUBR7851>
- [12] Chen D., Chen L. & Qian Z. (2022). Impact of pavement rutting on vehicle safety: A closed-loop assessment method. *Road Materials and Pavement Design*. <https://doi.org/10.1080/14680629.2022.2146601>
- [13] Federal Highway Administration (2014). *Distress Identification Manual for the Long-Term Pavement Performance Program*. Publication No. FHWA-HRT-13-092.
- [14] Setiawan D. M. (2020). The role of temperature differential and subgrade quality on stress, curling, and deflection behavior of rigid pavement. *Journal of the Mechanical Behavior of Materials*, 29(1), 94-105. <https://doi.org/10.1515/jmbm-2020-0010>
- [15] Sharifi N. P. & Mahboub K. C. (2018). Application of a PCM-rich concrete overlay to control thermal induced curling stresses in concrete pavements. *Construction and Building Materials*, 183, 502-512. <https://doi.org/10.1016/j.conbuildmat.2018.06.179>

- [16] Ramadhan R. H. & Al-Abdul Wahhab H. I. (1997). Temperature variation of flexible and rigid pavements in eastern Saudi Arabia. *Building and Environment*, 32(4), 367-373. [https://doi.org/10.1016/S0360-1323\(96\)00072-8](https://doi.org/10.1016/S0360-1323(96)00072-8)
- [17] Williamson R. H. (1977). Effect of environment on pavement temperature. *Proceedings of Third International Conference on Structural Design of Asphalt Pavements*, 1, 144-157.
- [18] Joshi A. P., Mehta Y. A., Cleary D., Henry S. & Cunliffe C. (2012). Load transfer efficiency of rigid airfield pavement relationship to design thickness and temperature curling. *Transportation Research Record: Journal of the Transportation Research Board*, 2300(1), 68-74. <https://doi.org/10.3141/2300>
- [19] Hunter R. N. (2017). Disproving bottom-up fatigue cracking in well-constructed asphalt pavements. *Proceedings of the Institution of Civil Engineers Construction Materials*, 170(CM4), 178-185. <http://dx.doi.org/10.1680/jcoma.16.00019>
- [20] Etheridge R. A., Wang Y. D., Kim S. S. & Kim Y. R. (2019). Evaluation of fatigue cracking resistance of asphalt mixtures using apparent damage capacity. *Journal of Materials in Civil Engineering*. [http://dx.doi.org/10.1061/\(ASCE\)MT.1943-5533.0002870](http://dx.doi.org/10.1061/(ASCE)MT.1943-5533.0002870)
- [21] Gopalam P., Debnath B. & Sarkar P.P. (2023). Effect of stabilized subgrade on rutting resistance of asphalt concrete pavement. Anjaneyulu M. V. L. R., HariKrishna M., Arkatkar S. S. & Veeraragavan A., *Recent Advances in Transportation Systems Engineering and Management. Lecture Notes in Civil Engineering*, 261. Springer, Singapore. https://doi.org/10.1007/978-981-19-2273-2_30
- [22] Epps J. & Monismith C. L. (1969). Influence of mixture variables on the flexural fatigue properties of asphalt concrete. *Journal of the Association of Asphalt Paving Technologists*, 38, 423-464.
- [23] Huang Y. H. (2004). *Pavement Analysis and Design*. Prentice Hall.
- [24] Brown R. B., Kandhal P. S., Roberts F. L., Kim Y. R., Lee D. Y. & Kennedy T. W. (2009). *Hot mix asphalt materials, mixture design, and construction*. NAPA Research and Education Foundation.
- [25] Mensching D. J., Rahbar-Rastegar R., Underwood B. S. & Daniel J. S. (2016). Identifying indicators for fatigue cracking in hot-mix asphalt pavements using viscoelastic continuum damage principles. *Transportation Research Record: Journal of the Transportation Research Board*, 2576, 28-39. <http://dx.doi.org/10.3141/2576-04>
- [26] Eslaminia M., Thirunavukkarasu S., Guddati M. N. & Kim Y. R. (2012). Accelerated pavement performance modeling using layered viscoelastic analysis. *The 7th RILEM International Conference on Cracking in Pavements*, Netherlands, pp. 497-506.
- [27] Park H. J., Eslaminia M. & Kim Y. R. (2014). Mechanistic evaluation of cracking in in-service asphalt pavements. *Materials and Structures*, 47(8), 1339-1358. <https://doi.org/10.1617/s11527-014-0307-6>
- [28] Mackiewicz P. (2018). Fatigue cracking in road pavement. *IOP Conference Series: Materials Science and Engineering*, 356, 012014. <https://doi.org/10.1088/1757-899X/356/1/012014>
- [29] McGennis R. B., Anderson R. M., Kennedy T. W. & Solaimanian M. (1994). *Background of Superpave asphalt mixture design and analysis*. Publication No. FHWA-SA-95-003. US Department of Transportation.
- [30] Roberts F., Kandhal P., Brown E., Lee D. & Kennedy T. (1996). *Hot Mix Asphalt Materials Mixture Design and Construction*. NAPA Education Foundation.
- [31] Jaskula P. (2014). Influence of compaction effectiveness on interlayer bonding of asphalt layers. *The 9th International Conference Environmental Engineering*, Vilnius.
- [32] Kim H., Arraigada M., Raab C. & Partl M. N. (2011). Numerical and experimental analysis for the interlayer behavior of double-layered asphalt pavement specimens. *Journal of Materials in Civil Engineering*, 23(1), 12-20. [https://doi.org/10.1061/\(ASCE\)MT.1943-5533.0000003](https://doi.org/10.1061/(ASCE)MT.1943-5533.0000003)
- [33] Mohammad L., Bae A., Elseifi M., Button J. & Patel N. Effects of pavement surface type and sample preparation method on tack coat interface shear strength. *Transportation Research Record: Journal of the Transportation Research Board*, 2180(1), 93-101. <https://doi.org/10.3141/2180-11>
- [34] Wang H. & Al-Qadi I. L. (2010). Near-surface pavement failure under multiaxial stress state in thick asphalt pavement. *Transportation Research Record: Journal of the Transportation Research Board*, 2154(1), 91-99. <https://doi.org/10.3141/2154-08>
- [35] Zhao Z., Xu L., Guan X., Li X. & Xiao F. (2022). Rutting and strain characteristics of rubberized asphalt pavement based on accelerated pavement tester. *Journal of Cleaner Production*, 376, 134219. <https://doi.org/10.1016/j.jclepro.2022.134219>
- [36] Dai X., Jia Y., Wang S. & Gao Y. (2020). Evaluation of the rutting performance of the field specimen using the hamburg wheel-tracking test and dynamic modulus test. *Advances in Civil Engineering*, 2020, 9525179. <https://doi.org/10.1155/2020/9525179>
- [37] Lv Q., Huang W., Sadek H., Xiao F. & Yan C. (2019). Investigation of the rutting performance of various modified asphalt mixtures using the Hamburg wheel-tracking device test and multiple stress creep recovery test. *Construction and Building Materials*, 206, 62-70. <https://doi.org/10.1016/j.conbuildmat.2019.02.015>
- [38] Rahman A. S. M. A., Larrain M. M. M. & Tarefder R. A. (2019). Development of a nonlinear rutting model for asphalt concrete based on Weibull parameters. *International Journal of Pavement Engineering*, 20(9), 1055-1064. <https://doi.org/10.1080/10298436.2017.1380807>

- [39] Singh P. & Swamy A. K. (2020). Probabilistic approach to characterise laboratory rutting behaviour of asphalt concrete mixtures. *International Journal of Pavement Engineering*, 21(3), 384-396. <https://doi.org/10.1080/10298436.2018.1480780>
- [40] Lee S. H., Vo H. V. & Park D. W. (2018). Investigation of asphalt track behavior under cyclic loading: Full-scale testing and numerical simulation. *Journal of Testing and Evaluation*, 46(3), 934-942. <https://doi.org/10.1520/JTE20160554>
- [41] Debnath B., Deb P. & Sarkar P. P. (2023). Effect of soil properties on the rutting performance of flexible pavement: A numerical study. Muthukkumaran K., Rathod D., Sujatha E. R. & Muthukumar M., *Transportation and Environmental Geotechnics. Lecture Notes in Civil Engineering*, 298. Springer, Singapore. https://doi.org/10.1007/978-981-19-6774-0_13